Human Molecular Genetics, 2020, Vol. 29, No. 18 3132–3144

doi: 10.1093/hmg/ddaa211
Advance Access Publication Date: 24 September 2020
General Article

GENERAL ARTICLE

FKBP8 variants are risk factors for spina bifida

Tian Tian[1,2,†], Xuanye Cao[2,†], Sung-Eun Kim[3], Ying Linda Lin[2], John W. Steele[2], Robert M. Cabrera[2], Menuka Karki[2], Wei Yang[4], Nicholas J. Marini[5], Ethan N. Hoffman[2], Xiao Han[2], Cindy Hu[3], Linlin Wang[1,†], Bogdan J. Wlodarczyk[2], Gary M. Shaw[4], Aiguo Ren[1,*,‡], Richard H. Finnell[2,6,*] and Yunping Lei[2,*,¶]

[1]Institute of Reproductive and Child Health, National Health Commission Key Laboratory of Reproductive Health, Peking University, Beijing 100191, China, [2]Center for Precision Environmental Health, Department of Molecular and Cellular Biology, Baylor College of Medicine, Houston, TX 77031, USA, [3]Department of Pediatrics, The University of Texas at Austin Dell Medical School, Austin, TX 78723, USA, [4]Department of Pediatrics, Stanford University School of Medicine, Stanford, CA 94305, USA, [5]Department of Molecular and Cellular Biology, California Institute for Quantitative Biosciences, University of California, Berkeley, CA 94720, USA and [6]Departments of Molecular and Human Genetics and Medicine, Baylor College of Medicine, Houston, TX 77031, USA

*To whom correspondence should be addressed. Tel: 010-8280 1182; Fax: +86-82801140; Email: renag@bjmu.edu.cn; Tel: 713-798-4363; Fax: +1-7137988181; Email: Richard.Finnell@bcm.edu; Yunping.Lei@bcm.edu

Abstract

Neural tube defects (NTDs) are a group of severe congenital malformations caused by a failure of neural tube closure during early embryonic development. Although extensively investigated, the genetic etiology of NTDs remains poorly understood. *FKBP8* is critical for proper mammalian neural tube closure. *Fkbp8*$^{-/-}$ mouse embryos showed posterior NTDs consistent with a diagnosis of spina bifida (SB). To date, no publication has reported any association between *FKBP8* and human NTDs. Using Sanger sequencing on genomic DNA samples from 472 SB and 565 control samples, we identified five rare (MAF $\leq$ 0.001) deleterious variants in SB patients, while no rare deleterious variant was identified in the controls ($P = 0.0191$). p.Glu140* affected FKBP8 localization to the mitochondria and created a truncated form of the FKBP8 protein, thus impairing its interaction with BCL2 and ultimately leading to an increase in cellular apoptosis. p.Ser3Leu, p.Lys315Asn and p.Ala292Ser variants decreased FKBP8 protein level. p.Lys315Asn further increased the cellular apoptosis. RNA sequencing on anterior and posterior tissues isolated from *Fkbp8*$^{-/-}$ and wildtype mice at E9.5 and E10.5 showed that *Fkbp8*$^{-/-}$ embryos have an abnormal expression profile within tissues harvested at posterior sites, thus leading to a posterior NTD. Moreover, we found that *Fkbp8* knockout mouse embryos have abnormal expression of *Wnt3a* and *Nkx2.9* during the early stage of neural tube development, perhaps also contributing to caudal specific NTDs. These findings provide evidence that functional variants of *FKBP8* are risk factors for SB, which may involve a novel mechanism by which *Fkbp8* mutations specifically cause SB in mice.

[†]Linlin Wang, http://orcid.org/0000-0002-2033-9277
[‡]Aiguo Ren, http://orcid.org/0000-0001-9115-5638
[¶]Yunping Lei, http://orcid.org/0000-0003-1504-0884
[†] These authors have equal contribution to the manuscript.
Received: April 27, 2020. **Revised:** September 13, 2020. **Accepted:** September 17, 2020

Introduction

Neural tube defects (NTDs) are a group of congenital malformations caused by the failure of neural tube closure during the first four weeks of human embryonic development (1). NTDs are one of the most severe malformations of newborns, with a prevalence among live births in the USA of 1 in 1200 and a worldwide prevalence ranging from 1 in 1000 to 3–5 in 1000 (2). Spina bifida (SB) and anencephaly are the two most common subtypes of NTDs, which affect the spine and brain, respectively.

NTDs are considered collectively to represent a collection of complex disorders with multiple etiologies, stemming from the multiple interactions of genetic and environmental factors (3). Providing women with periconceptional supplemental folic acid (FA) has been shown to significantly reduce the risk of having an NTD affected pregnancy (4). However, there are still a large number (>400 000 pregnancies per year) of NTD affected infants conceived and born annually, even in countries that employ mandatory FA fortification of the food supply. These are referred to as FA-resistant NTDs (4). Previous studies demonstrated that gene variants are major contributory factors to the etiology of FA-resistant NTDs (5). Naturally occurring as well as induced or targeted mutations in over 300 different genes resulted in mice with NTD phenotypes. These genes are in multiple different signaling pathways, including the Wnt/ planar cell polarity (PCP) (6–10), sonic hedgehog (SHH) (11) and mitochondrial folate metabolic pathways (12). At present, there have been only a few mouse NTD genes that have been explored as contributing to the risk factors for human NTDs. A large number of genes that are related to NTDs in the mouse still lack any evidence that they contribute to human NTD risks (13).

FKBP8, also known as FKBP38, is a member of the FK506-binding protein family, which has a conserved peptidyl prolyl *cis*/*trans*-isomerase (PPIase) domain (14). Unlike other members in this family, FKBP8 exhibits peptidyl prolyl *cis*-*trans* isomerase activity and does not bind to the immunosuppressant drug FK506 (Tacrolimus) or facilitate PPIase activity (15). FKBP8 contains several functional regions, including the FK506 binding domain, a three-unit tetratricopeptide-repeat (TPR) domain, a leucine zipper repeat, and the C-terminal transmembrane (TM) domain (16). The TPR domain primarily controls FKBP8 as it forms multimeric complexes with other proteins. The C-terminal TM domain helps FKBP8 anchor to the mitochondrial membrane and distribute predominantly within mitochondria (17). FKBP8 plays essential roles in multiple biological functions, such as protein folding and trafficking, serving as a co-chaperone of heat shock proteins (18–19). It is also involved in cell size regulation (20) and acts as the inhibitory mammalian target of rapamycin (mTOR) signaling (21). FKBP8 is also an important inhibitor of apoptosis, which it accomplishes by anchoring the anti-apoptotic proteins BCL2 and BCLXL to the mitochondrial membranes (22). Additionally, during murine embryonic development, *Fkbp8* controls neural cell fate through antagonism of SHH signaling, which is critical for proper neural tube closure (23–25).

Transgenic mouse models demonstrated that *Fkbp8* nullizygous embryos showed abnormal neural tube development, skeletal defects, including scoliosis, rib deformities, club foot and curled tail (26–27). However, the underlying mechanism by which inactivation of the *Fkbp8* gene actually initiates the adverse morphogenetic events leading to the expression of NTDs remains unclear. Wong and colleagues reported that *Fkbp8*$^{-/-}$ mice had an isolated and completely penetrant SB, which is both folate- and inositol-resistant. These investigators stated that the loss of *Fkbp8* leads to increasing apoptosis in the posterior neural tube and impaired dorso-ventral patterning (26). Shirane and colleagues reported that *Fkbp8* could regulate protrudin-dependent membrane recycling and neurite outgrowth. It was proposed that knocking out the *Fkbp8* gene leads to disorganized neuroepithelium formation of the dorsal root ganglia, and that this contributes to the SB phenotype (27). Cho and coworkers focused on the role of *Fkbp8* in controlling neural cell identity through its antagonism of the SHH pathway. They found that *Fkbp8* could control neural tube patterning through a *Gli2*- and *Kif3a*-dependent mechanism (24). It is interesting that all *Fkbp8*$^{-/-}$ mice showed the 'open neural tube' only in the posterior region of the embryo, whereas the anterior region showed no obvious abnormal phenotype. Developmentally, the phenotype of *Fkbp8*$^{-/-}$ mice was similar to their wildtype littermates until E9.5, which is well within the timeframe when the events of early neural tube development are well underway. The abnormal 'open' neural tube was clearly evident around E10.5 (26). These studies indicate that there may exist some time- and position-specific biological mechanism underlying the occurrence of SB in *Fkbp8*$^{-/-}$ mice. Moreover, all the evidence on establishing the association between *FKBP8* and NTDs has been from animal models, as there have been no previous reports of human SB patients with variants in the *FKBP8* gene.

In this study, we sought to establish human evidence for an association between *FKBP8* and SB, and further explore the underlying biological mechanisms that lead to this abnormal phenotype. To rigorously test our hypothesis, we initially performed Sanger sequencing on DNA samples from 472 SB affected fetuses and 565 unaffected controls. Three novel variants, one rare variant and one stop-gain variant were identified among the SB patients, while no deleterious variants were identified in the control cohort. We performed functional assays to determine the effect of the five deleterious variants on *FKBP8* function. We determined that the five mutations have different modifications on *FKBP8* function, impacting subcellular localization of *FKBP8*, protein level, its interaction with BCL2. Furthermore, we collected tissue from the anterior and posterior portions of *Fkbp8* null and wildtype embryos at both E9.5 and E10.5 to perform RNA sequencing. The results revealed that the *Fkbp8* gene inactivation may influence the normal expression of *Wnt3a* and *Nxk2.9* in the posterior region during the early stages of neural tube development.

Results

Five rare deleterious variants in *FKBP8* are associated with an increased risk for human SB

To examine the association between *FKBP8* variants with human NTDs, we performed Sanger sequencing on bloodspot derived DNA samples from 472 SB newborns and 565 non-malformed controls. Five rare variants (p.Glu140*, p.Ser3Leu, p.Ala251Gly, p.Ala292Ser and p.Lys315Asn) of the *FKBP8* gene were identified in five SB cases and none of these were detected in the controls (Table 1). Detailed information of the five SB cases is provided in Supplementary Material, Table S1. All of the NTD cases were diagnosed with lumbar SB. Two of the cases were white Hispanic, while three of them were non-Hispanic whites. Among the five mutations, p.Glu140* was a stop-gain mutation, while the other four variants were nonsynonymous mutations. Only p.Ser3Leu was reported in the gnomAD data with different MAF frequencies in Latino/AMR (MAF = 0.0004804, allele counts: 17/35384) and non-Finnish

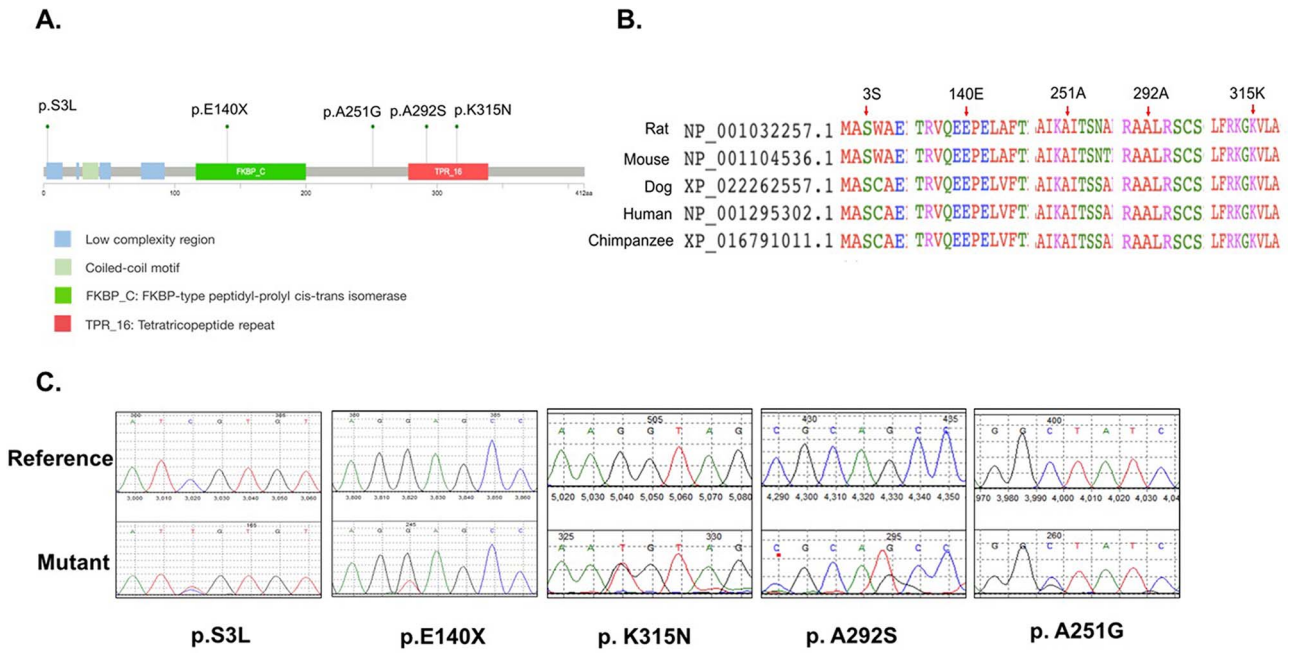

Figure 1. Identification of spina bifida-associated rare variants in the *FKBP8* gene. (**A**) Conserved domains of FKBP8 and positions of the five detected mutations. (**B**) Conservation estimation of identified variants between different species. (**C**) Sanger Sequencing results for the SB-cohort.

European (MAF = 0.00004001, allele counts: 5/124968), while others were not found in any available databases, indicating that those four mutants were novel mutations. All of those five variants were predicted as deleterious by PolyPhen and/or SIFT. As shown in Figure 1C, those variants were found to be heterozygous in individual SB cases. Amongst controls, we only identified a single mutation, c.260C>T(p.Ala87Val), with a MAF of 9%. Compared with our control data, the deleterious rare mutations of *FKBP8* showed a significant ($P = 0.0191$) enrichment in the SB group in our study. This enrichment is also significant ($P < 0.01$) when comparing to gnomAD data (Supplementary Material, Table S2). We also compared the enrichments of deleterious rare variants by ethnic groups. In our cohort, three variants were found in Hispanic NTD cases and two variants were in non-Hispanic NTD cases, but no such variants were found in either group of local controls. When compared with control data from public domain sources, we found an enhanced enrichment of rare deleterious variants in our local NTD cases than in Hispanic but not in non-Hispanic controls from the public domain (Supplementary Material, Table S3).

The amino acid at the position where the five mutants occurred is highly evolutionarily conserved among various species (Fig. 1B). The p.Ser3Leu mutation is located in the low complexity region of FKBP8, which is a potential transcriptional activation domain of the protein. The stop-gain mutation p.Glu140* is localized in the FKBP-type peptidyl-prolyl *cis-trans* isomerase region. The p.Ala251Gly, p.Ala292Ser and p.Lys315Asn sites are in the TPR motif of the FKBP8 protein, which primarily orchestrates the formation of multimeric complexes between FKBP8 and other proteins and helps FKBP8 anchor to the membrane and to mitochondria (17) (Fig. 1A).

The variants impaired subcellular localization of FKBP8 and its protein levels

We initially examined the effect of these variants on FKBP8 subcellular localization. The constructs of *FKBP8* (WT and mutants) were overexpressed in HeLa cell lines. As shown in Figure 2A, wildtype FKBP8 was primarily located in the mitochondria with no expression in the nucleus. Compared with wildtype, p.Ser3Leu, p.Ala251Gly, p.Ala292Ser and p.Lys315Asn didn't affect the location of FKBP8. However, the p.Glu140* caused an obvious mislocalization of FKBP8, as it was now no longer restricted to the mitochondrion, but was also expressed in the nucleus. The quantified results were consistent with the imaging, demonstrating that the abnormal location of the FKBP8 protein in p.Glu140* group was significantly higher than in the wildtype group (Fig. 2B). Western blotting assay was performed to investigate the effect of the variants on the FKBP8 protein levels. As a result, the protein of variants p.Ser3Leu, p.Lys315Asn and p.Ala292Ser were less abundant than were the wildtype FKBP8 ($P < 0.05$), indicating that those variants may decrease the FKBP8 expression or damage its protein stability (Fig. 2D). The p.Glu140* mutant showed a shorter band around 40 kDa, indicating it produced a truncated form of FKBP8 protein (Fig. 2C).

The variants affected FKBP8 co-localization with BCL2 and its interaction with *BCL2*

Previous studies reported that *FKBP8* interacted with *BCL2* and co-localized with BCL2 protein in the mitochondria (17). Therefore, we tested the effect of the variants on the co-localization of FKBP8 and BCL2 by co-transfecting *BCL2* and *FKBP8* constructs (WT and mutants) into Hela cells, and then performed immunostaining assays. As depicted in Figure 3A, BCL2 was mainly expressed in the mitochondria. The wildtype FKBP8 and BCL2 were co-localized in the mitochondria. Compared with the wildtype FKBP8 group, the p.Glu140* mutant failed to co-localize with BCL2 and showed an irregular nucleus. Other variants did not impair the co-localization of BCL2 with FKBP8. However, the cells transfected with p.Ser3Leu and p.Lys315Asn *FKBP8* constructs showed flattened, longer and irregular shaped nuclei, indicating the co-transfection of

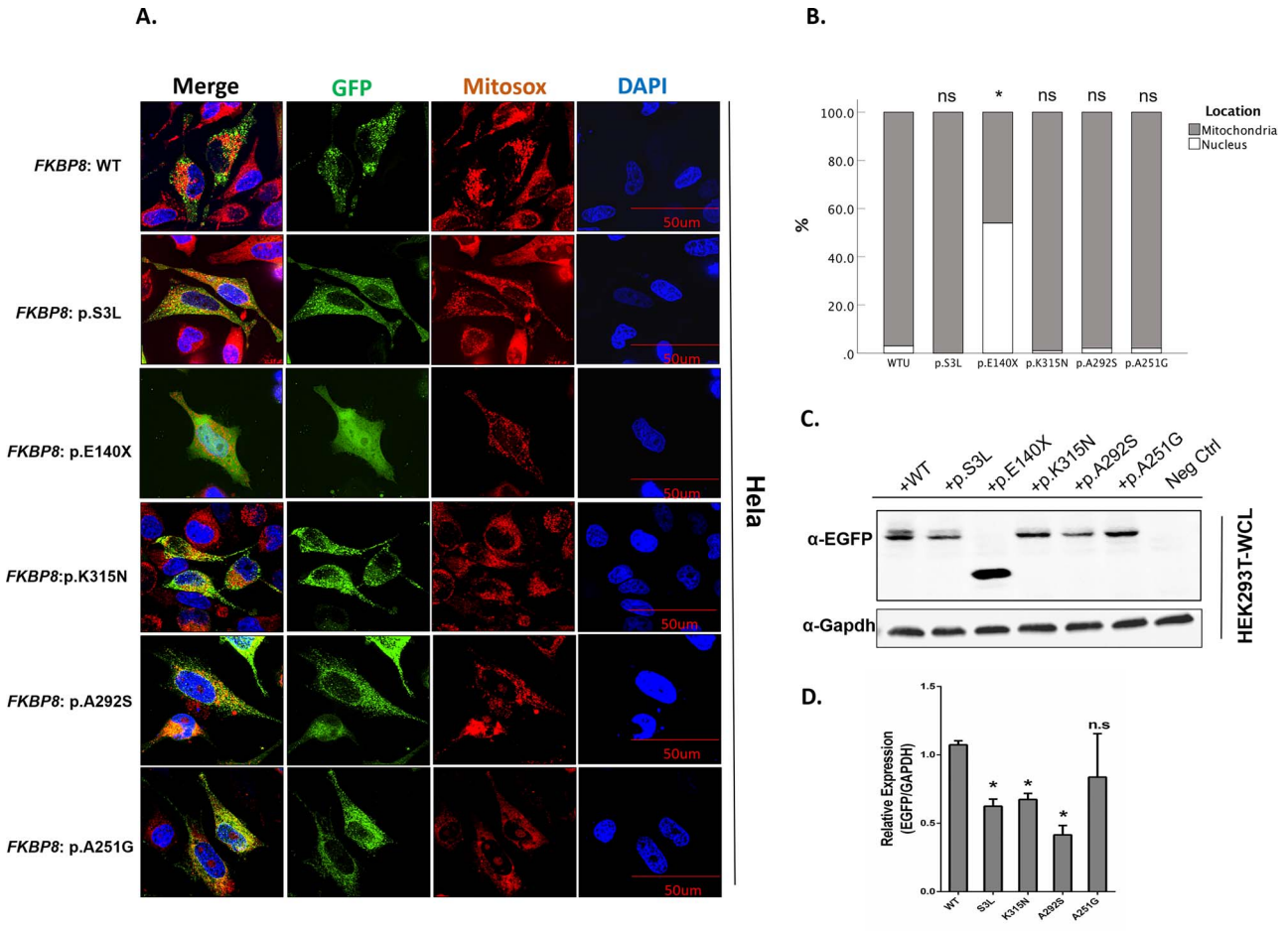

Figure 2. Rare variants affected FKBP8 subcellular localization and protein level. (**A**) HeLa cells were transfected with mutated and wildtype constructs of GFP-tagged *FKBP8* for 48 h incubation and then were imaged under a deconvolution microscope. GFP signaling was used to show the location of FKBP8, while Mitosox was stained to show the location of mitochondria. (**B**) Ten fields of view were chosen randomly and about 200 cells in each group were counted. The percentage of abnormal localized cells in mutant groups was compared with wildtype group by using Pearson χ^2-test Ns: no significant difference. Asterisk indicates the p.E140X variant resulted in more cells with mislocalized expression than occurring in the wildtype cells. (**C**) Western blot assay was performed in HEK293T overexpression model. (**D**) The western blotting assay was repeated three times and student *t*-test was performed to compare the protein level between the mutated group with that of the wildtype group.

variants *FKBP8* p.Ser3Leu/p.Lys315Asn and *BCL2* alters or impairs protein localization and may compromise the integrity and functioning of these cells (Fig. 3A, quantitative analysis was shown in Supplementary Material, Figure S1). With respect to the statistical analyses, we primarily counted the numbers of cells with FKBP8 variants that failed to co-localize with BCL2 in the mitochondria. As a result, the rate of mis-co-localized cells in the p.Glu140* group was significantly higher than in the wildtype group (Fig. 3B). Co-IP assays in HEK293T cells were performed to examine the interaction between FKBP8 and BCL2 (Fig. 3C). The results showed that FKBP8 wildtype, p.Ser3Leu, p.Lys315Asn, p.Ala251Gly and p.Ala292Ser could interact with BCL2 normally, while the p.Glu140* variant did not bind to BCL2, demonstrating that this variant had impaired interactions with BCL2 (Fig. 3D).

The variants influenced cell apoptosis

FKBP8 is reported to be an essential antagonist of SHH signaling pathway and an important molecule in central nervous system development. Loss of *Fkbp8* causes ectopic and ligand-independent activation of the SHH pathway, leading to the expansion of ventral cell fates in the posterior neural tube and suppression of eye development (25). Given our long-standing interest in neural tube closure defects, we examined how *FKBP8* variants regulate SHH signaling activity by using the Gli responsive luciferase (Gli-Luc) reporter system. To our surprise, the western blotting revealed that the variants did not affect the expression of any of the tested SHH pathway proteins (Supplementary Material, Fig. S2A). Moreover, it turned out that there is no significant difference in the relative expression of Gli between wildtype and the mutated groups of FKBP8 (Supplementary Material, Fig. S2B).

We also examined whether the variants affected cell apoptosis by using TUNEL assays in HEK293T cells. When transfected with the *FKBP8* plasmids, the cells did not display obvious evidence of apoptosis (Supplementary Material, Fig. S3). However, when we co-transfected *FKBP8* (WT or mutants) and *BCL2* plasmid into cells, the transfected cells showed significant evidence of apoptosis. Compared with the *BCL2* only transfected group, *FKBP8* wildtype significantly decreased the level of apoptosis, indicating that *FKBP8* has an inhibitory effect on cellular apoptosis. Compared with the wildtype *FKBP8* group, p.Ser3Leu, p.Ala251Gly and p.Ala292Ser showed a decreased level of apoptosis, while p.Glu140* and p.Lys315Asn showed a significant increase in the amount of apoptosis observed (Fig. 4). These

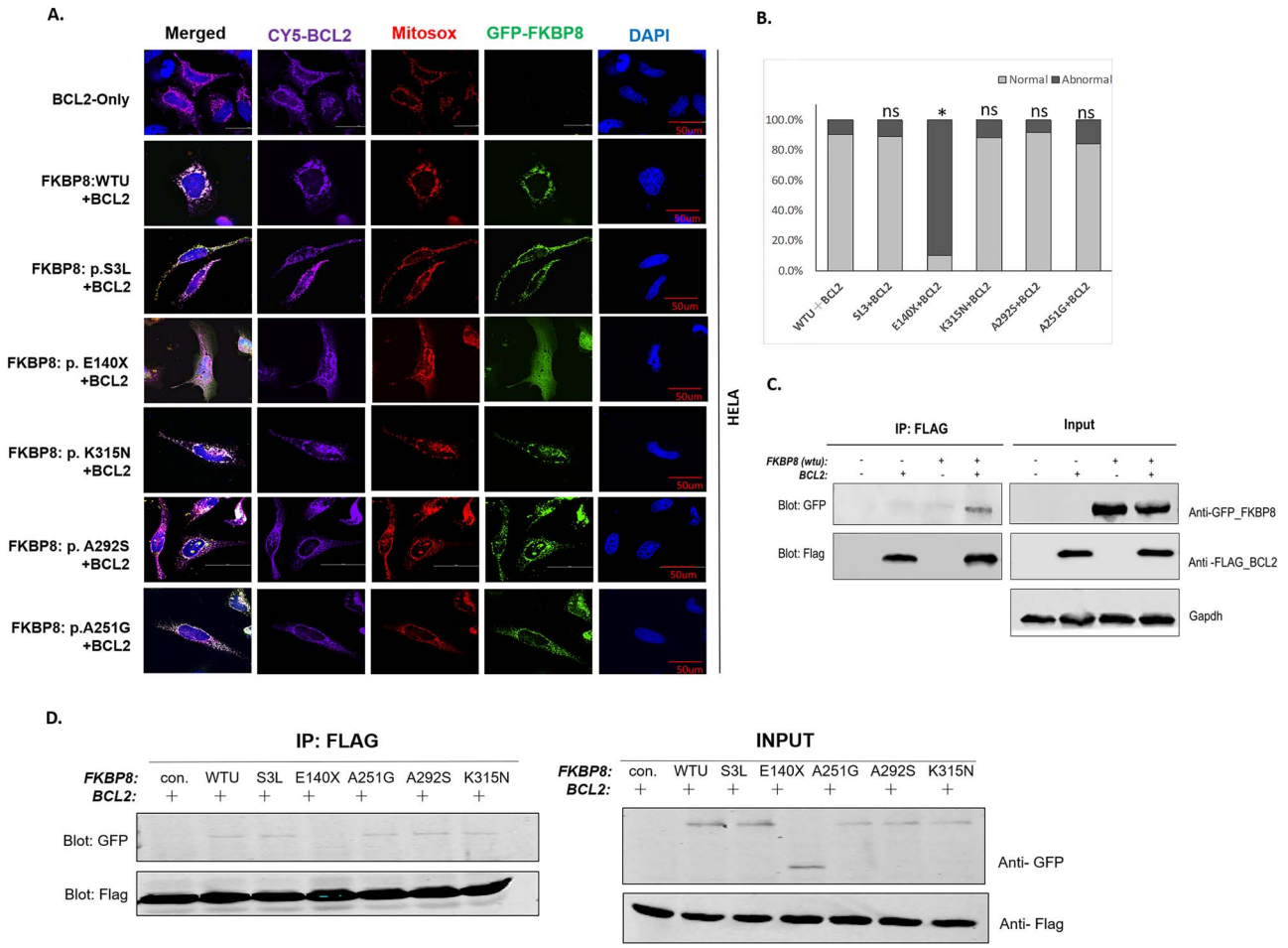

Figure 3. The co-localization of BCL2 and FKBP8 and the interaction between FKBP 8 and BCL2. (**A**) HeLa cells were co-transfected with mutated and wildtype constructs of FKBP8 and Flag-BCL2 plasmid for 48 h incubation and then were imaged under a deconvolution microscope. (**B**) Ten fields of view were chosen randomly and approximately 200 cells in each group were counted. The percentage of abnormal localized cells in mutant groups was compared with the wildtype group by using Pearson χ^2-test. *$P < 0.05$. Normal: both FKBP8 and BCL2 co-localize in mitochondria; abnormal: FKBP8 or BCL2 failed to locate in mitochondria. (**C**) Co-IP assay showed that wildtype of FKBP8 had interaction with BCL2 in HEK293T overexpression model. (**D**) Co-IP assay on mutant constructs of FKBP8 and BCL2.

results indicate that the identified variants have a significant impact on cellular apoptosis.

Gene expression analysis in the *Fkbp8* knockout mice

Our previous study found that neural tube closure in the *Fkbp8*$^{-/-}$ mice proceeds in a comparable manner as observed in their wildtype littermates at E9.5. However, the nullizygous mice showed obvious edema in the posterior neural tubes by E10.5 (26), whereas the anterior region remains normal and closed (Fig. 5A). In order to explore the underlying mechanism, we collected both posterior and anterior tissue from *Fkbp8*$^{-/-}$ and wildtype embryos at E9.5 and E10.5 for RNA sequencing. The posterior portion of the E9.5 and E10.5 embryos was dissected by cutting distal to the forelimb bud (Fig. 5A).

At E9.5, only 10 differentially expressed genes (DEGs) at the posterior site between *Fkbp8*$^{-/-}$ and wildtype embryos were identified (Fig. 5B). The number of DEGs at the posterior site increased to 210 at E10.5 (Fig. 5B), indicating that knockouts of *Fkbp8* gene may cause time- and position-specific abnormal expression of targeted genes. Moreover, there may exist driver gene(s) that are differentially expressed at E9.5 that influences the E10.5 gene expression profiles. Among the 10 DEGs in E9.5 embryos, *Wnt3a* and *Nkx2.9* were the top two candidate genes (Fig. 5C). Compared with the wildtype, *Wnt3a* expression in *Fkbp8*$^{-/-}$ mouse embryos showed an increased trend from E9.5 to E10.5 at the posterior site, while in the wildtype, its expression level decreased from E9.5 to E10.5 (Fig. 5D). The *Nkx2.9* gene was highly expressed only in *Fkbp8* null embryos in the posterior region at both E9.5 and E10.5 (Fig. 5E). At E10.5, gene ontology (GO) analysis found that DEGs of the posterior site tissues were mainly enriched in the cell fate commitment pathway, axon genesis and other neurodevelopment related pathways (Fig. 6A). Most of these genes showed increased expression in the null mice (Fig. 6B).

Discussion

FKBP8 is an important member of the family of intracellular receptors for the immunosuppressive drug FK506. Genetically inactivating the *Fkbp8* gene in mouse embryos resulted in a 100% penetrant defect in neural tube closure in the thoraco-lumbar-sacral region (26,28), indicating that *Fkbp8* plays a crucial role in neural tube closure (24,27–28). At present, there are no published studies reporting any genetic association of *FKBP8* with human NTDs, especially SB. In this study, we observed for the first time

A.

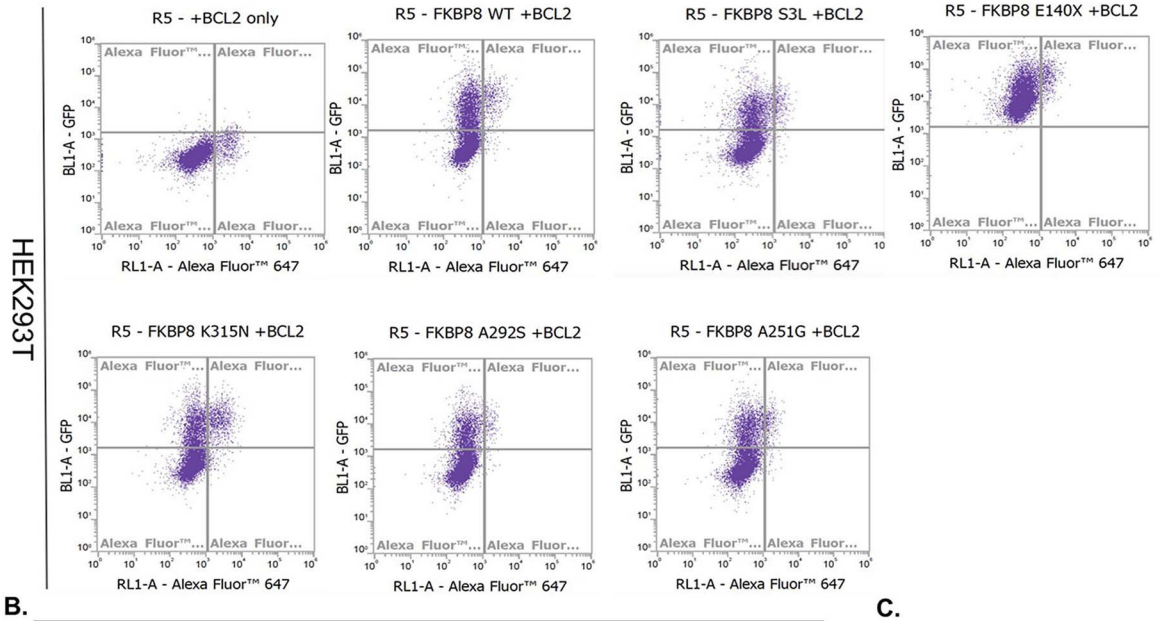

B.

Sample	Alexa Fluor 647-/GFP+(1)		Alexa Fluor 647+/GFP+(1)		Total	*p*1	*p*2
	N	%	N	%			
BCL2 ONLY	9380	94.6	535	5.4	9915	<0.001	
FKBP8 WT +*BCL2*	9726	95.8	423	4.2	10149	-	<0.001
FKBP8 S3L +*BCL2*	9266	97.3	269	2.7	9891	0.001	<0.001
FKBP8 E140X +*BCL2*	9400	95.5	450	4.5	9892	0.047	0.019
FKBP8 K315N +*BCL2*	8938	91.1	870	8.9	9808	<0.001	<0.001
FKBP8 A292S +*BCL2*	9747	98.5	153	1.5	9900	<0.001	0.031
FKBP8 A251G +*BCL2*	9510	97.2	272	2.8	9782	0.146	<0.001

C.

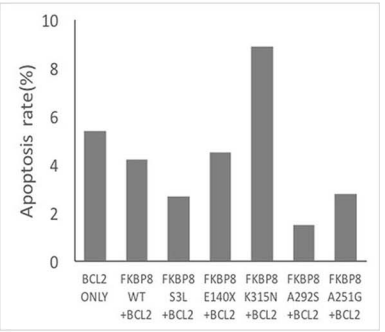

Figure 4. The influence of *FKBP8* variants on apoptosis. (**A**) The HEK293T cells were transfected with *BCL2* constructs along with *FKBP8* (WT or mutant) and then cultured for 48 h. TUNEL assay and flow cytometry was carried on to test the cellular apoptosis. (**B**) The rates of the apoptosis of each group were counted. Pearson χ^2 analysis was performed to compare the apoptosis rate between groups. p1: *P*-value when compared with *FKBP8* wildtype and *BCL2* co-transfected group. p2: *P*-value when compared with *BCL2* only transfected group. $P < 0.05$ represents a significant difference. (**C**) Bar chart of the apoptosis rate of each group.

a stop-gain mutation (p.Glu140*) and four novel/rare deleterious missense variants of *FKBP8* in SB infants. As Table 2 indicates, the five identified variants had various effects on on the biological function of FKBP8. p.Glu140* formed a truncated version of FKBP8 that was mislocalized from anchoring to mitochondria to being expressed within the nucleus. The variants p.Ser3Leu, p.Ala292Ser and p.Lys315Asn significantly decreased the FKBP8 protein levels. These results indicate that rare deleterious variants of *FKBP8* may contribute to the etiology of human SB, which support the results found in mouse studies (26–27). As all five of these variants were heterozygous in patients, we assume they may interact with other genetic variants or environment factors to contribute to the observed SB phenotype.

BCL2, an integral inner mitochondrial membrane protein, is a critical regulator of apoptosis (29). Previous studies reported that BCL2 could block apoptotic death through diverse pathways (30). It is well known that *FKBP8* is associated with the *BCL2* gene. A previous study found that FKBP8 was associated with BCL2 and BCLXL in immunoprecipitation assays, and co-localized with these proteins in the mitochondria to block apoptosis (17). It is reported that $Ca2^+$/calmodulin can bind to FKBP8 and form a $Ca2^+$/calmodulin/FKBP8 complex, which can activate BCL2 function and thereby participate in the regulation of apoptosis in neuronal tissues (15). Moreover, Shirane *et al.* (27) generated *Fkbp38*$^{-/-}$ mice and found an increased frequency of apoptosis and aberrant migration of neuronal cells, thus leading to a SB phenotype in mice. In the present study, we hypothesized that the rare variants may inhibit neural tube closure by impairing the interaction between FKBP8 and BCL2, leading to the mislocation of BCL2 and subsequently influence the rate of cellular apoptosis. We determined using a subcellular co-localization assay that the p.Glu140* variant failed to co-localized with BCL2 into the mitochondria. The Co-IP assay showed that p.Glu140* impaired the interaction between FKBP8 with BCL2. Moreover, the apoptosis assay showed that compared with wildtype, the p.Glu140* variant of FKBP8 increased the cellular apoptosis rate. These findings imply that p.Glu140* of *FKBP8* may form a truncated body of the FKBP8 protein, subsequently impairing its interaction with BCL2, and causing the failure of BCL2 to anchor to the mitochondria, compromising normal cellular apoptosis. We also noticed that in the subcellular location assay, the cells being transfected with

A.

B.

Embryonic Day	Ratio is	DEG numbers ($^{ad}P<0.1$)
9.5	P_KO vs P_WT	12
9.5	CA_KO vs CA_WT	3
9.5	CA_WT vs P_WT	0
9.5	CA_KO vs P_KO	107
10.5	P_KO vs P_WT	210
10.5	CA_KO vs CA_WT	13
10.5	CA_WT vs P_WT	807
10.5	CA_KO vs P_KO	1252

C.

Gene	log²FoldChange	ad-p
Fkbp8	-5.86203	5.02E-129
Nkx2.9	3.03508	0.003697
Wnt3a	-1.70252	0.004682
Ccnd2	0.71673	0.034547
Zfp738	-0.89972	0.043598
Olig2	2.46939	0.058412
Aqp11	-1.66230	0.058412
Lhx3	3.25778	0.061113
Orc6	-0.40915	0.061113
Armc6	0.74199	0.098437

D.

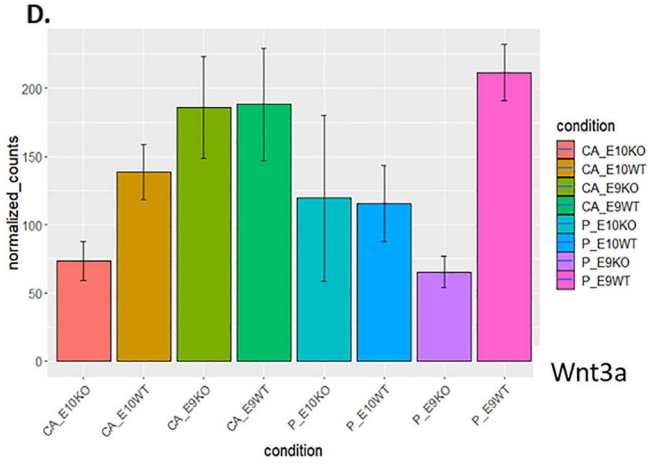

E.

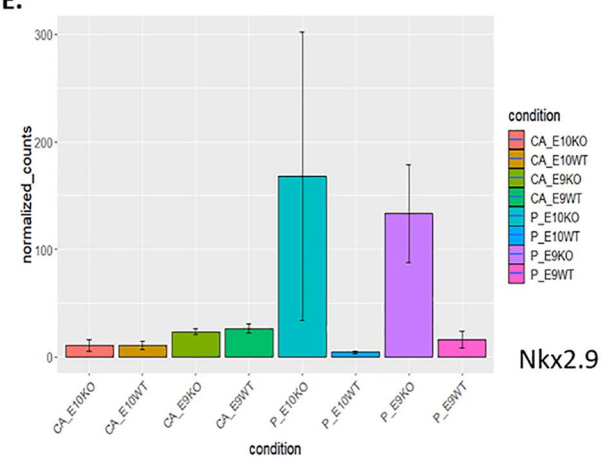

Figure 5. The KO mice showed an abnormal time-and position-specific RNA expression profile. (**A**) The phenotype of the mouse embryo at E9.5 and E10.5. The red lines represent the schematic that indicates the region of tissue microdissected. (**B**) Differentially expressed gene numbers match phenotypes. (**C**) Differently expressed genes at the posterior site between Fkbp8 null mice and wildtype mice at E9.5. (**D**) The expression profile of *Wnt3a* gene. (**E**) The expression profile of *Nkx2.9* gene. CA: head parts; P: posterior part. (**F**) Protein expression of Wnt3a in E10.5 mice embryo. (**G**) Protein expression of Nkx2.9 in E10.5 mice embryo.

FKBP8 p.Lys315Asn showed irregular nuclei, indicating that this variant may actually induce cellular apoptosis. This result was validated by the apoptosis assay, in which p.Lys315Asn had a significantly increased rate of apoptosis. The results indicate that p.Lys315Asn induces cell apoptosis and may lead to impairment in neural tube closure. However, the variant

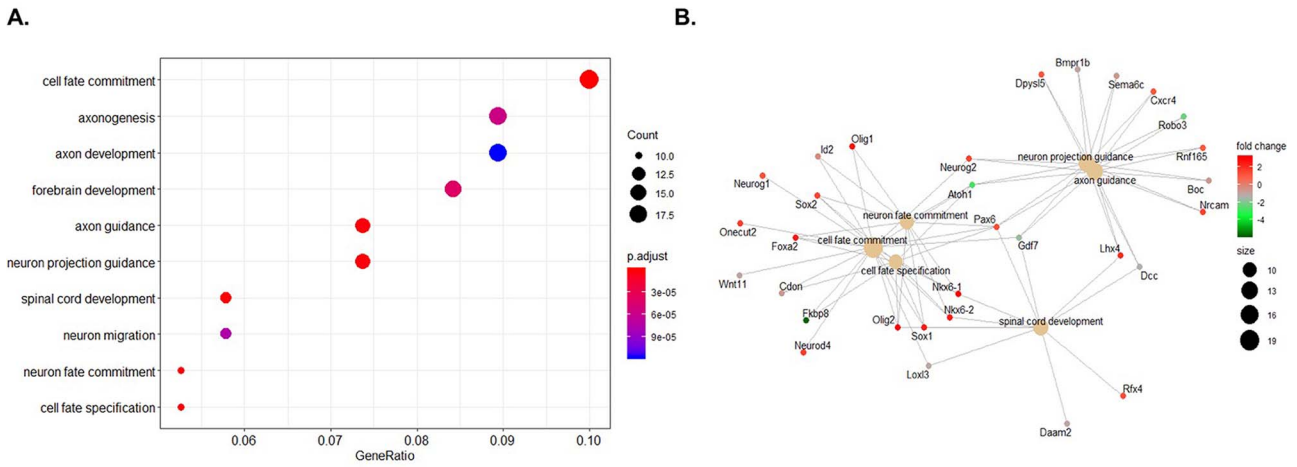

Figure 6. GO analysis of differentially expressed genes in E10.5. (**A**) Dot plot demonstrates that top 10 dysregulated classification in the cellular process. (**B**) Network analysis of genes included in the top 10 dysregulated classification.

FKBP8 p.Ala292Ser which locates in the same domain as p.Lys315Asn had an opposite effect on cell apoptosis. One possible explanation is that the characteristic of the amino acid changing direction is not the same between A292S and K315N. Alanine (A) is hydrophobic while serine (S) is polar uncharged; however, lysine (K) is positively charged while asparagine (N) is also a polar uncharged amino acid. Different amino acid characteristic changes may be one of the reasons for the variants in same FKBP8 protein domain producing opposite results with respect to apoptosis. This is not a unique observation in the NTD field. Previously, we described both gain and loss of function variants in LRP6 genes that were associated with SBs (31) using a mouse Lrp6 model system (32–33). Therefore, it is possible that both loss of function and gain of function variants in the FKBP8 gene may contribute to the increased risk of SB, but this hypothesis should be rigorously tested in the future using Fkbp8 gain of function mouse models. Another explanation for why those suspected gain-of-function variants (p.S3L, p.A251G and p.A292S) could increase the risk of SB is that they may contribute to other function loss of FKBP8/Fkbp8 that was not explored in this study, although they may not be a risk factor in causing apoptosis.

Previous mouse models have demonstrated that all *Fkbp8* nullizygous mice presented with isolated posterior NTDs, specifically SB at embryonic day 18.5, indicating a strong association between *Fkbp8* with neural tube closure (26–28). However, the morphogenetic changes secondary to the *Fkbp8* knockout leading to the NTD phenotype in mice remains unclear. It is interesting that our previously published work on this mouse model revealed that during the early stage of neural tube closure (E9.5), the *Fkbp8*$^{-/-}$ embryos are indistinguishable from their wildtype littermates. However, the null embryos all have 'open' posterior neural tubes when they are examined after E10.5 (26). There was abnormal expression of the FKBP8 protein in the posterior portions of the embryo, extending from the thoracic to lumbar regions, whereas protein expression in the anterior region remains normal. Based on the previous findings, we assumed that there may exist genes that are causative for caudal but not cranial NTDs in the *Fkbp8* KO mouse model. Further, we hypothesized that there may exist different gene expression profiles between the early and later stages of neural tube closure in these embryos. In this study, the RNA-seq data clearly demonstrated a significant difference in the gene expression profiles between E9.5 and E10.5 in the posterior regions of the embryo. The numbers of DEGs at the posterior site between WT and *Fkbp8*$^{-/-}$ group significantly increased from E9.5 to E10.5. This finding was consistent with our previously published mouse study in which the *Fkbp8*$^{-/-}$ null embryos only showed abnormal phenotypes after E10.5 (26). The RNA-seq study provides evidence that *Fkbp8* $^{-/-}$ may cause abnormal gene expression in the early stage of neural tube development, thus driving different expression profiles at E10.5 within the posterior neural tube.

Among the 10 DEGs identified at E9.5, *Wnt3a* and *Nkx2.9* were two of the most significantly differently expressed genes. Wnt3a is an important member of Wnt/β-catenin signaling pathway and is highly expressed in the dorsal neural tube which will give rise to the neural crest in *Xenopus*, zebrafish, and mice (34). The neural crest formation in whole embryos is inhibited when the activity of Wnt3a is blocked, suggesting that Wnt3a had a critical role in patterning the neural tube along its dorso-ventral axis (35). It is also reported that this kind of inducing effect happened in an early developmental stage when the neural plate is forming (36). All previous studies supported our finding that Wnt3a had limited expression in the posterior portion of E9.5 *Fkbp8*$^{-/-}$ mice. Therefore, we assume that the loss of *Fkbp8* may decrease the expression of Wnt3a in the posterior regions of the embryo, thus impairing the proper patterning of the neural tube leading to an SB defect in the nullizygous mice. *Nkx2.9* (known as *NKX2.8* in humans) is collectively orthologous with *Nkx2.2* (37). Although there is no direct evidence of an association between *Nkx2.9* with neural development, *Nkx2.2* acts downstream of *SHH* signaling pathway and upstream of *Lmx1b* in a signaling cascade that directs the development, specification, and differentiation of 5-HT (5-hydroxytryptamine) neurons in the central nervous system in mice (38). Additionally, it is important to note that as a downstream transcription factor of SHH signaling, the expression of *Nkx2.2* is expanded dorsally in *FKBP8* nullizygous embryos (25,39). In our previous study, we performed microarray analyses and determined that *Fkbp8* knockout mice had a higher expression of *Nkx2.9* (26). In the current study, we further validated this finding, suggesting that an *Fkbp8* knockout would up-regulate *Nkx2.9* expression. Moreover, the *Fkbp8* knockout mouse only had specifically high expression of *Nkx2.9* at the

Table 1. Information of the detected FKBP8 mutations in SB DNA samples

Position	Variant	Protein change	SNP ID	Function	SIFT score	PolyPhen Score	ExAC Frequency	GenomeAD Frequency	Ethnicity
Chr19:18648482	c.874 G>T	p. A292S	/	Nonsynonymous	Damaging	Probably damaging	0	0	White Hispanic
Chr19:18648411	c. 944 G>T	p. K315N	/	Nonsynonymous	Damaging	Probably damaging	0	0	White Hispanic
Chr19:18649046	c.752 C>G	p. A251G	/	Nonsynonymous	Damaging	Probably damaging	0	0	non-Hispanic white
Chr19:18652773	c.8 C>T	p. S3L	rs543806511	Nonsynonymous	Damaging	Probably damaging	3.138e-05	7.87E-05	non-Hispanic white
Chr19:18650405	c.420 G>T	p.E140X	/	Stop gain	/	/	0	0	non-Hispanic white

posterior site, perhaps explaining the presence of NTDs only in this portion of the embryo.

At E10.5, GO analysis found that the DEGs of the posterior embryo are primarily enriched for genes in the cell fate commitment pathway, axon genesis, and other neurodevelopment related pathways. Previous studies found that apoptosis plays a major role in shaping the developing nervous system during embryogenesis, as neuronal precursors differentiate to become postmitotic neurons. *In utero*, neural precursor cells (NPCs) are produced in excessive numbers and differentiate into postmitotic neurons. Following this period of excessive proliferation, the unneeded NPCs and neurons would be selectively eliminated during a period of substantial cell death by apoptosis (40). Given that our previous research found that *Fkbp8*$^{-/-}$ embryos showed increased apoptosis at the posterior site at E10.5, the abnormal expression of cell fate determinants, as well as axonal genesis genes may disrupt the normal progress of neural cell differentiation, resulting in activating apoptosis and inducing posterior NTDs in mice. The GO analysis also indicated that the *Fkbp8*$^{-/-}$ mouse could be another model of the failed NTD closure secondary to precocious neuronal differentiation, similar to the miR302$^{-/-}$ mouse model (41).

In conclusion, in this study, we demonstrated for the first time an association between *FKBP8* variants and increased risk for SB in a human cohort by identifying five rare deleterious *FKBP8* variants in NTD-affected infants. These variants had a range of physiological influences on FKBP8 protein function. The *Fkbp8* KO mouse model in this study also demonstrated that *Fkbp8* knockout may disrupt the normal expression of *Wnt3a* and *Nkx2.9* at posterior site, which may lead to the observed posterior NTD. This study provides novel insight into the mechanisms underlying the development of NTDs in this unique mouse model. Further human genomic studies are warranted that involve NTDs-trios in order to explore the origins of the *FKBP8* variants. Moreover, further functional experiments on mice to examine how abnormal expression of *Wnt3a* and *Nkx2.9* interrupt neural tube development will be necessary to understand the underlying molecular pathogenesis of the *FKBP8* knockout mouse.

Materials and Methods

Study population and Sanger sequencing

Human newborn screening bloodspot samples were collected from a case-control study conducted by the California Birth Defect Monitoring Program (42). Included for this study were 472 singleton infants with SB (cases) and 565 unrelated healthy infants with matched ancestry as controls. Among these samples, 192 SB and the 565 controls were collected between 1983 and 1999. Additional 280 SB samples were recruited from August 2009 to November 2012 through a web-based outreach program supported by 32 SB Association chapters and 61 SB specialty practices within the USA, as previously described (43). The cases were from two independent largely Caucasian population cohorts. In total, 81.8% of subjects of the first cohort were non-Hispanic white and 62.1% of the subjects of the second cohort were of Hispanic descent. We checked the frequencies of the rare variants of *FKBP8* gene in Hispanic and non-Hispanic population in public databases (i.e. GnomAD database). No significant difference was observed between the two populations ($P = 0.607$). Thus, we assume that the genetic background of the two populations was generally consistent and merged them together in our analysis.

Table 2. Summary of cell functional assay

	p.S3L	p.E140X	p.A251G	p.A292S	p.K315N
Location of FKBP8	Normal	Abnormal	Normal	Normal	Normal
FKBP8 protein level	↓	Truncated	–	↓	↓
Co-localization with BCL2	normal	Abnormal	normal	normal	normal
Interaction with BCL2	–	↓	–	–	–
Apoptosis	↓	↑	–	↓	↑
SHH signaling pathway	–	–	–	–	–

Notes: ↓: down-regulated; ↑: up-regulated; –: no significant influence.

DNA was extracted from the newborn screening bloodspots using the Puregene DNA Extraction Kit (Qiagen,Valencia, CA) and amplified using the GenomiPhi Kit (GE Healthcare, Marlborough, MA). *FKBP8* (Accession #: NM_012181.5) Sanger sequencing was performed using an ABI3730 DNA Analyzer. Primers for both PCR amplification and sequencing are provided in Supplementary Material, Table S4. All samples were obtained with approval from the State of California Health and Welfare Agency Committee for the Protection of Human Subjects. This study was approved by University of Texas at Austin (IRB approval number: 2014120041) where the work was initially conducted.

Plasmids

pcDNA-3.1(+)-N-eGFP-*FKBP8* (clone ID: Z26522) was purchased from Genscript (https://www.genscript.com/). *FKBP8* p.Ser3Leu, p.Glu140*, p.Ala251Gly, p.Ala292Ser and p.Lys315Asn were produced by the Genescript company based on the pcDNA-3.1(+)-N-eGFP-*FKBP8* wildtype vector. The construct of Flag-*Bcl2* was a gift from Clark Distelhorst (Addgene, ID:18003) (44).

Cell culture and transfection

HeLa cells (human cervical cancer), HEK293T and NIH3T3 cells were grown in Dulbeco's Modified Eagles's Medium (DMEM, Gibco™) supplemented with 10% heat-inactivated fetal bovine serum (FBS, Gibco™) and 1% Antibiotic-Antimycotic (Gibco™). Cultures were maintained at 37°C in a humidified atmosphere containing 5% CO_2. Cell transfection was carried out using Lipofectamine2000 (Invitrogen™, CA, USA) according to the manufacturer's protocol. The transfection efficiency was shown in Supplementary Material, Figure S4. We performed qPCR to determine the expression of the plasmid, which was shown in Supplementary Material, Figure S5.

Immunofluorescence

HeLa cells were plated at a density of 3×10^5 cells per ml onto 18 mm cover slips (Corning, NY, USA) for 20 h before transfection. For *FKBP8* subcellular localization, 1.5 μg mutant and wildtype of *FKBP8* vectors were transfected into cells. After culturing for 48 h, the cells were fixed with 4% paraformaldehyde on coverslips for 5 min and then rinsed with 1% PBS. DAPI (300 ng/ml, Invitrogen™) was used to stain the nucleus for 2 min. For co-localization of FKBP8 and BCL2, 1.0 μg *FKBP8* plasmid and 0.75 μg *BCL2* plasmid were co-transfected into cells. After 48 h, the mitochondrion of cells was stained by MitoSOX™ Red reagent (Invitrogen™) according to the manufacturer's protocol. The cells were fixed with 4% paraformaldehyde on coverslips for 20 min and rinsed with 1% PBS. Cell membranes were permeabilized with 1% Triton X-100. Cells were blocked in 3% BSA for 1 h and then incubated in rabbit anti-Flag antibody (1:800, Cell Signaling Technology, USA, D6W5B) overnight. A secondary antibody was used (1:2000; Alexa Fluor 647, Life Technologies) to stain the cells for 1 h. Cells were finally stained with DAPI (300 ng/ml, Invitrogen™) for 2 min. Images were taken by using a deconvolution microscope (Nikon T2). Image data were quantified using ImageJ software. Statistical analyses were performed using SPSS 20.0 software (IBM Company, USA). The staining assay was performed in both HEK293T and Hela cells twice.

Western blotting assay

HEK293T cells were transfected with GFP-tagged *FKBP8* (WT or mutants) and cultured for 48 h. Cells were rinsed with cold 1% PBS twice and then lysed with 1x NP40 Lysis buffer (Invitrogen™) with cOmplete™ ULTRA Tablets (Millipore Sigma) for 20 min. The proteins were immunoblotted with anti-GFP (1:500, Cell Signaling), anti-GAPDH (1:1000, Cell Signaling, Danvers, MA, 2218S), anti-FLAG (1:1000, Cell signaling Technology, USA, D6W5B), anti-SUFU (C81H7, Cell Signaling, Danvers, MA), anti-PTCH1 (2468 T, Cell Signaling, Danvers, MA), anti-GLI1 (Cell Signaling, Danvers, MA), anti-GLI3 (Cell Signaling, Danvers, MA), anti-SHH (Cell Signaling, Danvers, MA) overnight. IRDye® 800CW goat anti-rabbit IgG secondary antibodies (LI-COR,Cambridge, UK) were used to incubate the cells for 1 h. The images were captured by Odyssey® (LI-COR). Each western blotting assay was performed in triplicate.

Co-immunoprecipitation

HEK293T cells were transfected with the Flag-tagged *BCL2* construct and GFP-tagged *FKBP8* constructs (WT or mutants). Cells were cultured for 48 h and then were washed with PBS and lysed by rocking in RIPA lysis buffer in 4°C for 20 min. The protein concentration was determined by the use of a Bradford assay. For IP process, the total lysates were incubated with Anti-FLAG® M2 Magnetic Beads (Millipore) with a concentration of 2 μg per μg protein in a cold room for 16 h, then the beads were washed with RIPA buffer three times and finally boiled in 1x SDS loading buffer. Lysed samples were loaded onto an 8–16% PAGE gel. Nitrocellulose membranes were used for Western blotting. After 1 h blocking, anti-rabbit-GFP (1:500), anti-rabbit-GAPDH (1:1000, Cell Signaling, Danvers, MA, 2218S) and anti-Flag (1:1000, Cell signaling Technology, USA, D6W5B) were used to incubate the membrane overnight in 4°C. IRDye® 800CW goat anti-rabbit IgG secondary antibodies (LI-COR, Cambridge, UK) were used at 1:10 000, and protein bands were analyzed on Odyssey® (LI-COR). The co-immunoprecipitation was repeated twice.

TUNEL assay

HEK293T cells were transfected with different groups of *FKBP8* constructs (wt or mutants), or co-transfected with *BCL2* plasmid

and *FKBP8* in six-well plates. Cells were cultured for 48 h and TUNEL assay was performed by using Click-iT™ Plus TUNEL Assay Kit (C10619, Invitrogen) according to manufacturer's protocol. Cell flow cytometry was performed by using the Cell Sorter Sony SH800 system to detect cell apoptosis. The TUNEL assay was performed twice.

Luciferase assay

NIH3T3 cells were plated in 24-well plates and grown until 50–60% confluence. Each well was subsequently transfected with 200 ng Gli-luc and 40 ng SV40-Renilla plasmids along with *FKBP8*-GFP (WT or mutants). The cells were lysed 48 h post-transfection, and the luciferase activity was measured using a Dual Luciferase Assay Kit (Promega, Madison, WI). The Biotek-2 plate reader was used to read the luminescence activity. For the Luciferase assay, we used three samples for each group and repeated the experiment three times.

RNA sequencing and analysis

Tissue was harvested from both posterior and anterior portions of the *Fkbp8* knockout mice and wildtype mouse embryos at E9.5 and E10.5. Total RNA was extracted using the Quick-RNA MicroPrep Kit (Zymo Research, CA, USA). The concentration and integrity of the RNA were measured by Nanodrop2000 (Thermofisher, Waltham, MA). The library was prepared using the NEBNext Ultra RNA with Poly-A selection kit and was sequenced on an Illumina Hi-Seq 4000 (Admera Health LLC, South Plainfield, NJ). Differential gene expression was determined with fold change > 1.5 and $P < 0.05$ genes with > 1 count per million. Any gene with a *P*-value greater than false discovery rate, after Benjamini–Hochberg correction for multi-testing, was deemed significantly differentially expressed under the test conditions as compared to the controls.

Bioinformatics and statistical analysis

The Mutation Surveyor Software (SoftGenetics, LLC) was used to blast the sample and reference sequencing. A variant was designated as a novel if it was not found in the ExAC (Exome Aggregation Consortium) or GnomAD databases (https://gnomad.broadinstitute.org/). The potential pathogenic effect of the missense variants on protein function was predicted using online programs: PolyPhen V2 (Polymorphism Phenotyping) (http://genetics.bwh.harvard.edu/pph2/) and SIFT (Sorting Intolerant From Tolerant) (https://sift.bii.a-star.edu.sg). The conservation estimations were performed by using online software Cluster Omega (https://www.ebi.ac.uk/Tools/msa/clustalo/). All parameters were set at the website's recommendations. The localization of the variants in their protein domains was assessed by Uniprot (http://www.uniprot.org/). RNA-seq data analysis was performed by using kallisto and DEseq2 (45). Gene set enrichment analysis (GSEA) is carried out by using javaGSEA2–3.0 (46).

All data (mean ± SE) were analyzed with a Student's *t*-test, and *P*-values < 0.05 were considered statistically significant. *FKBP8* mutation enrichment was determined using Fisher's exact test compared to the public databases and control populations in our study (variants with MAF < 0.001 were counted).

Supplementary Material

Supplementary Material is available at *HMG* online.

Acknowledgments

We thank the Breast Center Pathology Core, and Pathology & Histology Core of Baylor College of Medicine for helping with the histology assays. This project was supported by grants from NIH (HD081216, HD083809 and HD100535 to Drs. Finnell and Lei, HD067244 to Dr Finnell, and HD093758 to Drs. Finnell and Kim). Dr Richard Finnell was supported in part by funds made available from the William T. Butler M.D. Distinguished Chair endowment at Baylor College of Medicine. We thank the California Department of Public Health, Maternal Child and Adolescent Health Division for providing surveillance data from California for this study. The findings and conclusions in this report are those of the authors and do not necessarily represent the official position of the California Department of Public Health. The authors acknowledge the Texas Advanced Computing Center at The University of Texas at Austin for providing high-performance computing resources that have contributed to the research results reported within this paper. URL: http://www.tacc.utexas.edu.
Conflict of Interest statement. Dr Richard Finnell formerly held a leadership position with and Drs.Cabrera andWlodarczykwere formerlymembers of the now dissolved TeratOmic Consulting LLC.

Author contributions

Y.L., A.R. and R.H.F. conceived and designed the experiments. Y.L., T.T., X.C. and E.H. generated and analyzed sequencing data. T. T., X.C., S.E.K, R.M.C., C.H., X.H. and M.K. performed cell-based functional analysis. W.Y., G.M.S W.L.L. and R.H.F. identified case and control bloodspots and acquired clinical data. Y.L.L, J.W.S and B.J.W worked on mice related assays. X.C., T.T. and Y.L. worked on RNAseq and data analysis. T.T., X.C. and Y.L. drafted the manuscript, and all other authors assisted in editing.

References

1. Wallingford, J.B., Niswander, L.A., Shaw, G.M. and Finnell, R.H. (2013) The continuing challenge of understanding, preventing, and treating neural tube defects. *Science*, **339**, 1222002.
2. Avagliano, L., Massa, V., George, T.M., Qureshy, S., Bulfamante, G.P. and Finnell, R.H. (2019) Overview on neural tube defects: from development to physical characteristics. *Birth. Defects. Res.*, **111**, 1455–1467.
3. Wilde, J.J., Petersen, J.R. and Niswander, L. (2014) Genetic, epigenetic, and environmental contributions to neural tube closure. *Annu. Rev. Genet.*, **48**, 583–611.
4. Copp, A.J., Stanier, P. and Greene, N.D. (2013) Neural tube defects: recent advances, unsolved questions, and controversies. *Lancet Neurol.*, **12**, 799–810.
5. Copp, A.J. and Greene, N.D. (2010) Genetics and development of neural tube defects. *J. Pathol.*, **220**, 217–230.
6. Lei, Y., Zhang, T., Li, H., Wu, B.L., Jin, L. and Wang, H.Y. (2010) VANGL2 mutations in human cranial neural-tube defects. *N. Engl. J. Med.*, **362**, 2232–2235.
7. Chen, Z., Lei, Y., Cao, X., Zheng, Y., Wang, F., Bao, Y., Rui, P., Finnell, R.H., Zhang, T. and Wang, H. (2018) Genetic analysis of Wnt/PCP genes in neural tube defects. *BMC Med. Genet.*, **11**, 38.
8. Lei, Y., Kim, S.E., Chen, Z., Cao, X., Zhu, H., Yang, W., Gary, M.S., Zheng, Y., Zhang, T. and Wang, H. (2019) Variants identified

in PTK7 associated with neural tube defects. *Mol. Genet. Genomic. Med.*, **7**, e00584.
9. Kibar, Z., Bosoi, C.M., Kooistra, M., Salem, S., Finnell, R.H., De Marco, P., Elisa, M., Alexander, G., Valeria, C. and Philippe, G. (2009) Novel mutations in VANGL1 in neural tube defects. *Hum. Mutat.*, **30**, 706–715.
10. Kharfallah, F., Guyot, M.C., El Hassan, A.R., Allache, R., Merello, E., De Marco, P., Graziella, D.C., Valeria, C. and Kibar, Z. (2017) Scribble1 plays an important role in the pathogenesis of neural tube defects through its mediating effect of Par-3 and Vangl1/2 localization. *Hum. Mol. Genet.*, **26**, 2307–2320.
11. Murdoch, J.N. and Copp, A.J. (2010) The relationship between sonic hedgehog signaling, cilia, and neural tube defects. *Birth Defects Res. A Clin. Mol. Teratol.*, **88**, 633–652.
12. Kim, J., Lei, Y., Guo, J., Kim, S.E., Wlodarczyk, B.J., Cabrera, R.M., Ying, L., Nilssond, T.K., Zhang, T. and Ren, A. (2018) Formate rescues neural tube defects caused by mutations in Slc25a32. *Proc. Natl. Acad. Sci. USA*, **115**, 4690–4695.
13. Greene, N.D. and Copp, A.J. (2014) Neural tube defects. *Annu. Rev. Neurosci.*, **37**, 221–242.
14. Lam, E., Martin, M. and Wiederrecht, G. (1995) Isolation of a cDNA encoding a novel human FK506-binding protein homolog containing leucine zipper and tetratricopeptide repeat motifs. *Gene*, **160**, 297–302.
15. Edlich, F., Weiwad, M., Erdmann, F., Fanghanel, J., Jarczowski, F., Rahfeld, J.U. and Fischer, G. (2005) Bcl-2 regulator FKBP38 is activated by Ca2+/calmodulin. *EMBO J.*, **24**, 2688–2699.
16. De Cicco, M., Milroy, L.G. and Dames, S.A. (2018) Target of rapamycin FATC domain as a general membrane anchor: the FKBP-12 like domain of FKBP38 as a case study. *Protein Sci.*, **27**, 546–560.
17. Shirane, M. and Nakayama, K.I. (2003) Inherent calcineurin inhibitor FKBP38 targets Bcl-2 to mitochondria and inhibits apoptosis. *Nat. Cell Biol.*, **5**, 28–37.
18. Wang, X., Venable, J., LaPointe, P., Hutt, D.M., Koulov, A.V., Coppinger, J., Gurkan, C., Kellner, W. and Matterson, J. (2006) Hsp90 cochaperone Aha1 downregulation rescues misfolding of CFTR in cystic fibrosis. *Cell*, **127**, 803–815.
19. Walker, V.E., Atanasiu, R., Lam, H. and Shrier, A. (2007) Co-chaperone FKBP38 promotes HERG trafficking. *J. Biol. Chem.*, **282**, 23509–23516.
20. Rosner, M., Hofer, K., Kubista, M. and Hengstschlager, M. (2003) Cell size regulation by the human TSC tumor suppressor proteins depends on PI3K and FKBP38. *Oncogene*, **22**, 4786–4898.
21. Bai, X., Ma, D., Liu, A., Shen, X., Wang, Q.J., Liu, Y. and Jiang, Y. (2007) Rheb activates mTOR by antagonizing its endogenous inhibitor, FKBP38. *Science*, **318**, 977–980.
22. Shirane, M. and Nakayama, K.I. (2004) Immunophilin FKBP38, an inherent inhibitor of calcineurin, targets Bcl-2 to mitochondria and inhibits apoptosis. *Nihon Rinsho*, **62**, 405–412.
23. Fong, S., Mounkes, L., Liu, Y., Maibaum, M., Alonzo, E., Desprez, P.Y., Thor, A.D., Kashani-Sabet, M. and Debs, R.J. (2003) Functional identification of distinct sets of antitumor activities mediated by the FKBP gene family. *Proc. Natl. Acad. Sci. USA*, **100**, 14253–14258.
24. Cho, A., Ko, H.W. and Eggenschwiler, J.T. (2008) FKBP8 cell-autonomously controls neural tube patterning through a Gli2- and Kif3a-dependent mechanism. *Dev. Biol.*, **321**, 27–39.
25. Bulgakov, O.V., Eggenschwiler, J.T., Hong, D.H., Anderson, K.V. and Li, T. (2004) FKBP8 is a negative regulator of mouse sonic hedgehog signaling in neural tissues. *Development*, **131**, 2149–2159.
26. Wong, R.L., Wlodarczyk, B.J., Min, K.S., Scott, M.L., Kartiko, S., Yu, W., Merriweather, M.Y., Vogel, P., Zambrowicz, B.P. and Finnell, R.H. (2008) Mouse Fkbp8 activity is required to inhibit cell death and establish dorso-ventral patterning in the posterior neural tube. *Hum. Mol. Genet.*, **17**, 587–601.
27. Shirane, M., Ogawa, M., Motoyama, J. and Nakayama, K.I. (2008) Regulation of apoptosis and neurite extension by FKBP38 is required for neural tube formation in the mouse. *Genes Cells*, **13**, 635–651.
28. Tsurubuchi, T., Allender, E.V., Siddiqui, M.R., Shim, K.W., Ichi, S., Boshnjaku, V., Farnell, M.B., Xi, G., Finnell, R.H., Mclone, D.G. *et al.* (2014) A critical role of noggin in developing folate-nonresponsive NTD in Fkbp8 −/− embryos. *Childs Nerv. Syst.*, **30**, 1343–1353.
29. Fesus, L., Davies, P.J. and Piacentini, M. (1991) Apoptosis: molecular mechanisms in programmed cell death. *Eur. J. Cell Biol.*, **56**, 170–177.
30. Sasi, N., Hwang, M., Jaboin, J., Csiki, I. and Lu, B. (2009) Regulated cell death pathways: new twists in modulation of BCL2 family function. *Mol. Cancer Ther.*, **8**, 1421–1429.
31. Lei, Y., Fathe, K., McCartney, D., Zhu, H., Yang, W., Ross, M.E., Shaw, G.M. and Finnell, R.H. (2015) Rare LRP6 variants identified in spina bifida patients. *Hum. Mutat.*, **36**, 342–349.
32. Carter, M., Chen, X., Slowinska, B., Minnerath, S., Glickstein, S., Shi, L., Campagne, F., Weinstein, H. and Ross, M.E. (2005) Crooked tail (cd) model of human folate-responsive neural tube defects is mutated in Wnt coreceptor lipoprotein receptor-related protein 6. *Proc. Natl. Acad. Sci. USA*, **102**, 12843–12848.
33. Gray, J.D., Kholmanskikh, S., Castaldo, B.S., Hansler, A., Chung, H., Klotz, B., Singh, S., Brown, A.M. and Ross, M.E. (2013) LRP6 exerts non-canonical effects on Wnt signaling during neural tube closure. *Hum. Mol. Genet.*, **22**, 4267–4281.
34. Nordstrom, U., Jessell, T.M. and Edlund, T. (2002) Progressive induction of caudal neural character by graded Wnt signaling. *Nat. Neurosci.*, **5**, 525–532.
35. Saint-Jeannet, J.P., He, X., Varmus, H.E. and Dawid, I.B. (1997) Regulation of dorsal fate in the neuraxis by Wnt-1 and Wnt-3a. *Proc. Natl. Acad. Sci. USA*, **94**, 13713–13718.
36. Gunhaga, L., Marklund, M., Sjodal, M., Hsieh, J.C., Jessell, T.M. and Edlund, T. (2003) Specification of dorsal telencephalic character by sequential Wnt and FGF signaling. *Nat. Neurosci.*, **6**, 701–707.
37. Wang, C.C., Brodnicki, T., Copeland, N.G., Jenkins, N.A. and Harvey, R.P. (2000) Conserved linkage of NK-2 homeobox gene pairs Nkx2-2/2-4 and Nkx2-1/2-9 in mammals. *Mamm. Genome*, **11**, 466–468.
38. Ding, Y.Q., Marklund, U., Yuan, W., Yin, J., Wegman, L., Ericson, J., Deneris, E., Johnson, R.L. and Chen, Z.F. (2003) Lmx1b is essential for the development of serotonergic neurons. *Nat. Neurosci.*, **6**, 933–938.
39. Shirane-Kitsuji, M. and Nakayama, K.I. (2014) Mitochondria: FKBP38 and mitochondrial degradation. *Int. J. Biochem. Cell Biol.*, **51**, 19–22.
40. Hollville, E., Romero, S.E. and Deshmukh, M. (2019) Apoptotic cell death regulation in neurons. *FEBS J.*, **286**, 3276–3298.
41. Jacob, W.F., Hu, T.J. and Robert, B. (2018) Decoupling the impact of microRNAs on translational repression versus RNA degradation in embryonic stem cells. *elife*, **7**, e38014.
42. Croen, L.A., Shaw, G.M., Jensvold, N.G. and Harris, J.A. (1991) Birth defects monitoring in California: a resource

for epidemiological research. *Paediatr. Perinat. Epidemiol.*, **5**, 423–427.

43. Cao, X., Tian, T., Steele, J.W., Cabrera, R.M., Aguiar-Pulido, V., Wadhwa, S., Bhavani, N., Bi, P., Gargurevich, N., Hoffman, E. *et al.* (2020) Loss of RAD9B impairs early neural development and contributes to the risk for human spina bifida. *Hum. Mutat.*, **41**, 786–799.
44. Wang, N.S., Unkila, M.T., Reineks, E.Z. and Distelhorst, C.W. (2001) Transient expression of wild-type or mitochondrially targeted Bcl-2 induces apoptosis, whereas transient expression of endoplasmic reticulum-targeted Bcl-2 is protective against Bax-induced cell death. *J. Biol. Chem.*, **276**, 44117–44128.
45. Bray, N.L., Pimentel, H., Melsted, P. and Pachter, L. (2016) Near-optimal probabilistic RNA-seq quantification. *Nat. Biotechnol.*, **34**, 525–527.
46. Subramanian, A., Tamayo, P., Mootha, V.K., Mukherjee, S., Ebert, B.L., Gillette, M.A., Paulovich, A., Pomeroy, S.L., Golub, T.R., Lander, E.S. *et al.* (2005) Gene set enrichment analysis: a knowledge-based approach for interpreting genome-wide expression profiles. *Proc. Natl. Acad. Sci. USA*, **102**, 15545–15550.